Clinical Neurophysiology 131 (2020) 2460–2468

Contents lists available at ScienceDirect

Clinical Neurophysiology

journal homepage: www.elsevier.com/locate/clinph

Visualization of electrical activity in the cervical spinal cord and nerve roots after ulnar nerve stimulation using magnetospinography

Yuki Miyano [a], Shigenori Kawabata [b,*], Miho Akaza [c], Kensuke Sekihara [b], Yuko Hoshino [b], Toru Sasaki [d], Taishi Watanabe [a,d], SukChan Kim [a], Shinji Sato [a], Yuki Mitani [a], Yoshiaki Adachi [e], Atsushi Okawa [d]

[a] Healthcare Business Group, RICOH Company, Ltd., 2-3-10 Kandasurugadai Chiyoda-ku, Tokyo 101-0062, Japan
[b] Department of Advanced Technology in Medicine, Graduate School of Tokyo Medical and Dental University, 1-5-45 Yushima, Bunkyo-ku, Tokyo 113-8510, Japan
[c] Respiratory and Nervous System Science, Biomedical Laboratory Science, Graduate School of Medical and Dental Sciences, Tokyo Medical and Dental University, 1-5-45 Yushima, Bunkyo-ku, Tokyo 113-8510, Japan
[d] Department of Orthopaedic Surgery, Tokyo Medical and Dental University,1-5-45 Yushima, Bunkyo-ku, Tokyo 113-8510, Japan
[e] Applied Electronics Laboratory, Kanazawa Institute of Technology, Kanazawa-shi, Ishikawa 920-1331, Japan

ARTICLE INFO

Article history:
Accepted 14 July 2020
Available online 05 August 2020

Keywords:
Magnetoneurography
Magnetospinography
Evoked magnetic field
Somatosensory evoked potential
Ulnar nerve

HIGHLIGHTS

- We successfully obtained magnetospinography (MSG) measurements in spinal cord after ulnar nerve stimulation.
- Neural currents flow into the intervertebral foramina between C6/7 and T1/2.
- MSG with ulnar nerve stimulation at elbow is effective for lower cervical spinal cord activation.

ABSTRACT

Objective: To establish a method for magnetospinography (MSG) measurement after ulnar nerve stimulation and to clarify its characteristics.
Methods: Using a 132-channel magnetoneurography system with a superconducting quantum interference device, cervical MSG measurements were obtained for 10 healthy volunteers after stimulation of the ulnar nerve at the elbow and the wrist, and neural current distribution was calculated and superimposed on the cervical X-ray images.
Results: Neuromagnetic signals were obtained in all participants after applying the stimulus artifact removal algorithm. The measured magnetic field intensity after elbow stimulation was about twice that after wrist stimulation. Calculated neural currents flowed into the intervertebral foramina at C6/7 to T1/2 and propagated cranially along the spinal canal. The conduction velocity from the peak latency of inward currents at C5-C7 was 73.4 ± 19.6 m/s.
Conclusions: We successfully obtained MSG measurements after ulnar nerve stimulation. The neural currents flowed into the spinal canal from more caudal segments after ulnar nerve stimulation compared with median nerve stimulation, and these MSG measurements were effective in examining the spinal tracts at C5/6/7.
Significance: This is the first report on the use of MSG to visualize electrical activity in the cervical spinal cord and nerve root after ulnar nerve stimulation.

1. Introduction

Advances in diagnostic imaging modalities, such as magnetic resonance imaging (MRI), have led to progress in the morphological diagnosis of cervical cord compression lesions. In the elderly, due to the possibility of asymptomatic spinal cord compression (Matsumoto et al., 1998; Bednarik et al., 2008; Nagata et al.,

Abbreviations: CSP, common-mode subspace projection; DSSP, dual signal subspace projection; MSG, magnetospinography; SEP, somatosensory evoked potentials; SQUID, superconducting quantum interference device; UGRENS, unit gain constraint recursively applied null-steering spatial filtering.

* Corresponding author.
E-mail addresses: yuki.yh.hasegawa@jp.ricoh.com (Y. Miyano), kawabata.orth@tmd.ac.jp (S. Kawabata), mihonuro@tmd.ac.jp (M. Akaza), k-sekihara@nifty.com (K. Sekihara), hoshino.atm@tmd.ac.jp (Y. Hoshino), t-sasaki.orth@tmd.ac.jp (T. Sasaki), taishi.watanabe@jp.ricoh.com (T. Watanabe), sukchan.kim@jp.ricoh.com (S. Kim), shinji.s1.satoh@jp.ricoh.com (S. Sato), yuuki.ym.mitani@jp.ricoh.com (Y. Mitani), okawa.orth@tmd.ac.jp (A. Okawa).

https://doi.org/10.1016/j.clinph.2020.07.009
1388-2457/

2014; Nakashima et al., 2015), not only morphological but also neurofunctional information must be effectively obtained for the diagnosis of cervical cord disorders.

Conventional electrophysiological studies, such as somatosensory evoked potentials (SEP), are effective for detecting any conduction deficits in the cervical spinal cord, but not for detecting local conduction blocks. Similarly, needle electromyography can detect motor neuron anterior horn lesions, but is not suitable for examining the spinal tracts (white matter). Spinal cord evoked potentials are useful for detailed functional evaluation of spinal tracts, but may not be suitable as a preoperative test procedure due to the need to place recording electrodes in the epidural space or other sites close to the spinal cord (Shinomiya et al., 1988; Tani et al., 2000; Tamaki et al., 2007).

Neuromagnetic recording, which is hardly affected by the conductivity of surrounding tissue, provides higher spatial resolution compared with conventional electrical potential measurement and can be used to measure neural activity in the spinal cord and cauda equina, which are located deep from the body surface and surrounded by the spinal bone tissue (Ishii et al., 2012; Sumiya et al., 2017; Ushio et al., 2018). Sumiya et al. measured the spinal cord evoked magnetic field of the cervical spinal cord after median nerve stimulation and successfully visualized neural activities flowing through the intervertebral foramina at C4/5-Th1/2 into the spinal canal and ascending in the spinal canal. However, since the uppermost nerve roots forming the median nerve are located at C5 or C6, it is difficult to diagnose spinal tract disorders at C5/6 or lower levels using magnetospinography (MSG) with median nerve stimulation. The ulnar nerve, which originates from nerve roots at lower levels, would be theoretically more advantageous in the diagnosis of spinal cord disorders, but produces only a weak neural signal (Mackert et al., 2001). This has made it difficult to evaluate neural activity in the spinal canal with high spatial accuracy after ulnar nerve stimulation.

The aim of this study was to establish a method for MSG measurement using ulnar nerve stimulation and to clarify its characteristics in order to facilitate the diagnosis of spinal cord disorder at the C5/6 level and below.

2. Methods

2.1. Subjects

This study involved 10 healthy volunteers with no abnormal neurological findings (10 men; mean [± SD] age, 31.9 ± 6.0 years; height, 172.6 ± 5.6 cm; weight, 66.8 ± 13.0 kg; and BMI, 22.3 ± 3.4).

This study was approved by the ethics committee of Tokyo Medical and Dental University (approval No.: M2000-1229) and conducted in accordance with the Declaration of Helsinki. Written informed consent was obtained from all participants.

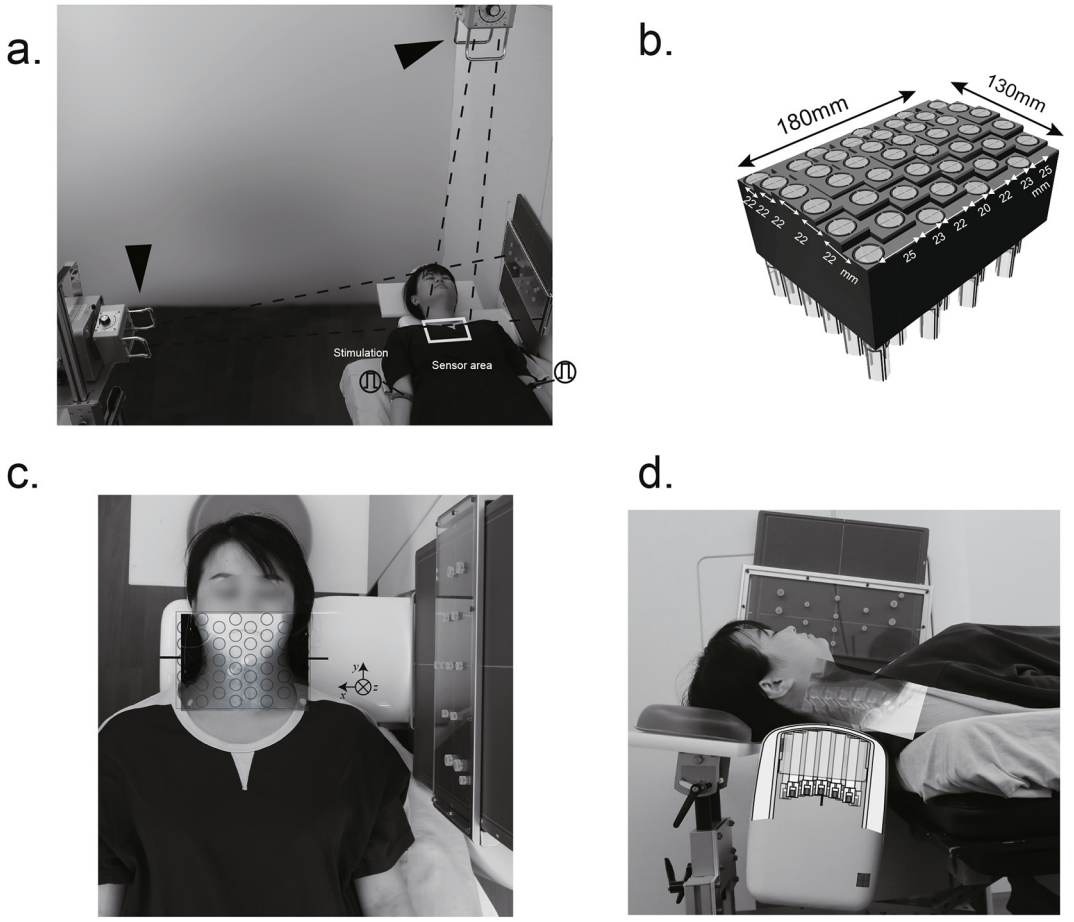

Fig. 1. Magnetoneurography system. (a) Measurement procedure. The participant was placed in the supine position with the back of the neck on the sensor area. Anteroposterior and lateral cervical plain X-rays were taken in the measurement position. (b) Superconducting quantum interference device (SQUID) sensor array. A total of 44 vector-type SQUID sensors are arranged in a 180 mm × 130 mm area. (c) Anteroposterior plain X-ray image taken in the measurement position with the vector sensor positions superimposed on a front-view photograph taken during measurement. (d) Lateral plain X-ray image taken in the measurement position with the sensor array then superimposed on a lateral-view photograph taken during measurement. The sensor array is curved to fit the lordosis of the cervical spine.

2.2. Measurement of evoked magnetic fields and somatosensory evoked potentials

All measurements were performed in a magnetically shielded room using the 132-channel superconducting quantum interference device (SQUID) magnetoneurography system co-developed by RICOH Company, Ltd., Kanazawa Institute of Technology, and Tokyo Medical and Dental University (Adachi et al., 2017). This system is equipped with 44 vector-type SQUID sensors that measure magnetic fields in three orthogonal directions in an array with an area of 180 mm × 130 mm. The sensor array surface is curved to fit to the lordosis of the cervical spine (Fig. 1).

Participants were placed in the supine position in a relaxed state and the C4 to Th2 vertebrae were located on the sensor array. Anteroposterior and lateral plain X-ray images were taken in the measurement position to determine the positional relationship between the cervical spine and the sensors.

The right and left ulnar nerves were electrically stimulated alternatively at the wrist with a stimulation frequency of 3–5 Hz and duration of 0.3 ms. Stimulus intensity was set to a supramaximal level by measuring SEP (EPi-EPc) at Erb's point, and SEP was simultaneously recorded during magnetic field measurement to confirm that the maximum SEP amplitude was maintained using an MEB-2312 system (Nihon Kohden Corporation, Japan).

The induced magnetic field was measured over the skin in the back of the neck with a bandpass filter of 100–5000 Hz and sampling rate of 40,000 Hz, and the measurements were averaged until the signal-to-noise (S/N) ratio was about 5 or higher (4000–8000 times).

The ulnar nerve was stimulated under the same conditions as those used for magnetic field measurement, and SEP was recorded from the C5 posterior-anterior surface electrode (C5S-AN) using the MEB-2312 system with a 10,000-Hz sampling rate and 20–3000-Hz bandpass filter and taking the average of 1000 responses. SEP recording was performed twice to confirm reproducibility.

The ulnar nerve was then stimulated at a supramaximal stimulus intensity at the elbow, and the induced magnetic field and SEP were measured at the neck using the same procedure.

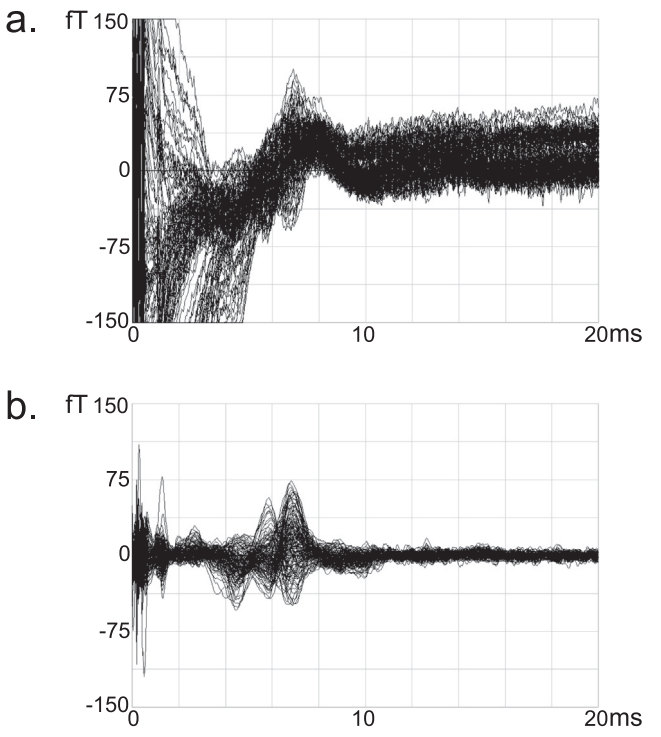

Fig. 2. Stimulation artifact removal by Dual signal subspace projection (DSSP) processing. (a) Original neuromagnetic fields after elbow stimulation. All waveforms of each sensor are superimposed. Since the stimulation artifacts overlap until approximately 10 ms after stimulation, the early latency neuromagnetic signals could not be evaluated. (b) Artifact removed from neuromagnetic fields after elbow stimulation. Stimulation artifacts were reduced and the neuromagnetic field could be evaluated from early latency.

2.3. Signal processing and electrical source estimation

Dual signal subspace projection (DSSP) was applied to measured magnetic field data to reduce artifacts due to electrical stimulation (Sekihara et al., 2016). Unit gain constraint recursively applied null-steering spatial filtering (UGRENS) was then applied to the magnetic field data after artifact removal in order to calculate the distribution of the neural currents in the neck

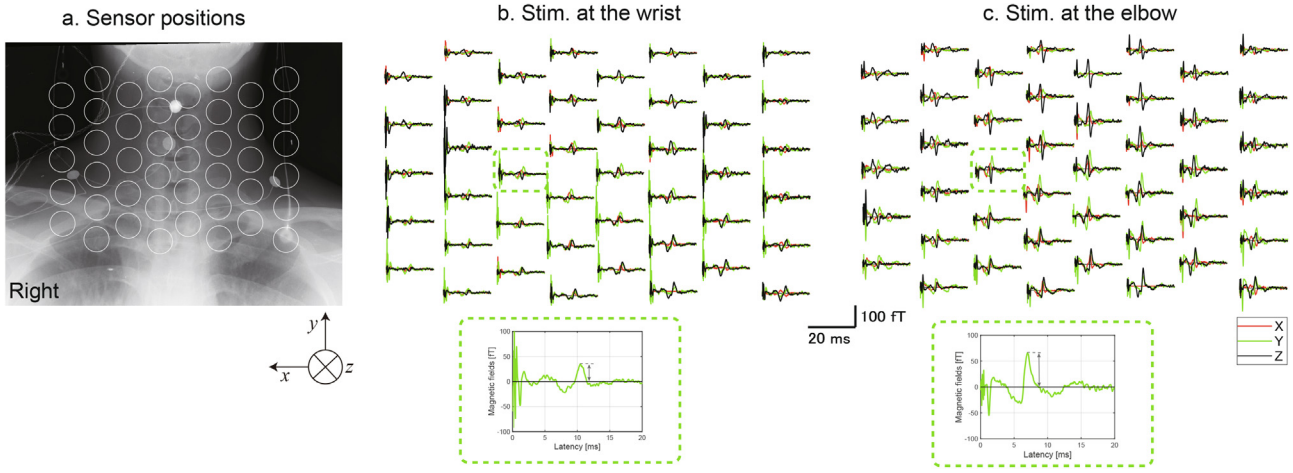

Fig. 3. Waveforms of the magnetic signal after artifact removal from each vector sensor. (a) Positions of the vector sensors superimposed on an X-ray image of the cervical spine. (b) Three-directional magnetic fields recorded by each vector sensor in response to left ulnar nerve stimulation at the wrist. Black traces are magnetic fields in the ventral–dorsal direction (Z axis; dorsal is upward in the graphs). Red traces are magnetic fields in the left–right direction (X axis; right is upward). Green traces are magnetic fields in the cranio–caudal direction (Y axis, cranial is upward). The lower panel shows the magnetic field waveform in the Y-axis direction of the vector sensor surrounded by the green dashed square. (c) Three-directional magnetic fields recorded by each vector sensor in response to left ulnar nerve stimulation at the elbow. The lower panel shows the waveform of the same Y-axis sensor as the one for wrist stimulation. Elbow stimulation produced a neuromagnetic field with an amplitude approximately twice that produced by wrist stimulation.

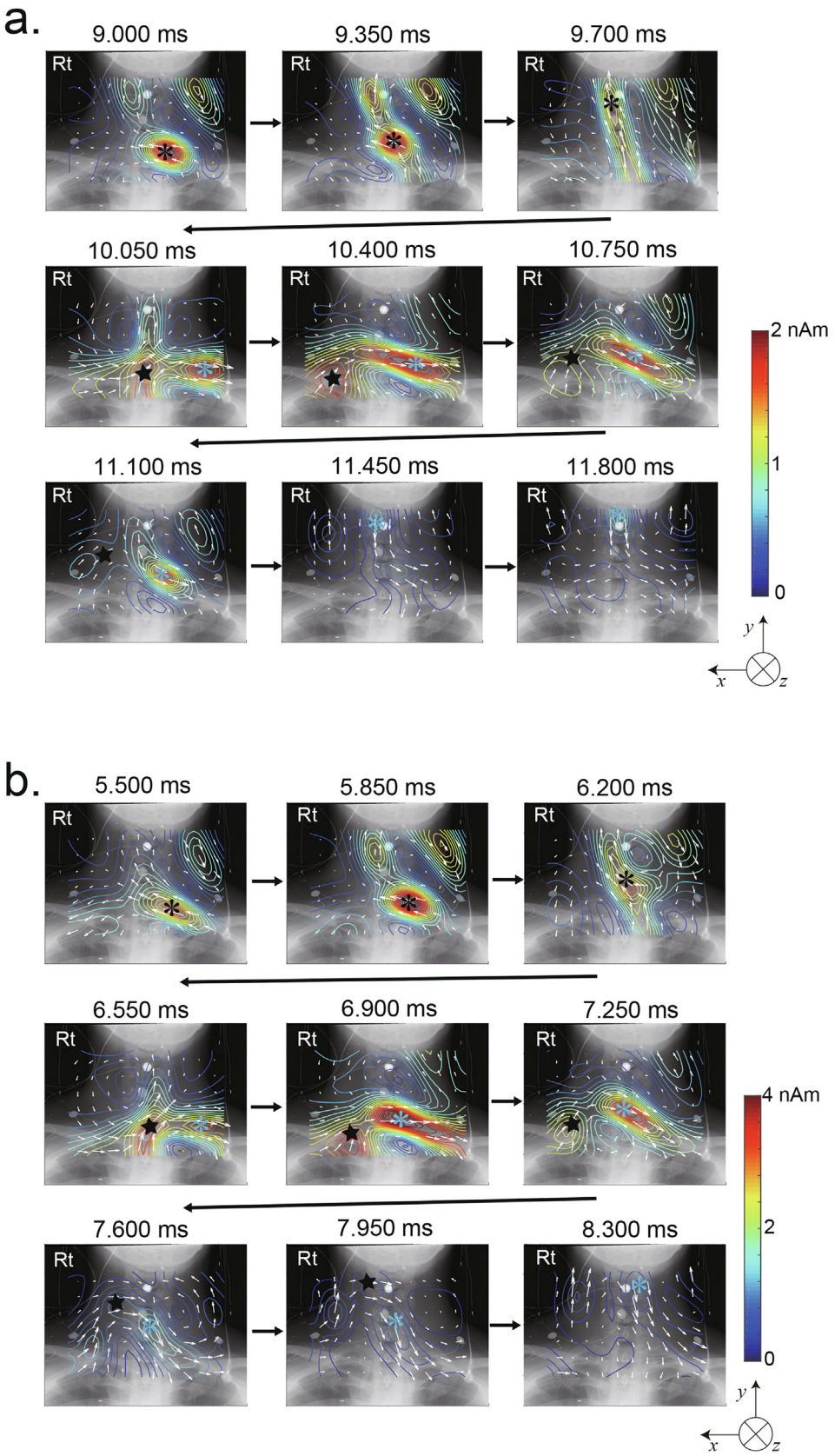

Fig. 4. Time course of neural current distribution in response to left ulnar nerve stimulation. (a) Wrist stimulation. (b) Elbow stimulation. Color indicates current density and white arrows show the direction and strength of currents on the XY plane. At first, leading components of the intra-axonal current appeared from the stimulated side and flowed into the intervertebral foramen and ascended along the spinal canal to the cranium ((a) 9.0–9.7 ms (b) 5.5–6.2 ms after stimulation, black asterisk). Subsequently, trailing intra-axonal currents appeared and propagated along the neural pathway ((a) 10.05–11.8 ms (b) 6.55–8.3 ms, light blue asterisk). Between the leading currents and the trailing currents, an inward current flowed perpendicular to the spinal canal and propagated cranially along the side of the spinal canal ((a) 10.05–11.1 ms (b) 6.55–7.95 ms, black star).

(Kumihashi et al., 2010; Sekihara et al., 2015). The region of interest was defined as the plane at the same depth as the vertebral canal obtained from a cervical lateral X-ray image taken in the measurement position (the distance in the Z-axis direction from the sensor is the same as that of the vertebral canal).

The calculated current distribution was superimposed on the X-ray images taken in the measurement position. Virtual electrodes were set at each vertebral and intervertebral level between C4/5 and Th1/2 to calculate current waveforms at each point. At a signal level equal to or less than the noise level (S/N ratio $\leq$ 1) was assigned a value of 0 to currents flowing into the intervertebral foramina.

To compare the distribution of the current flowing into the intervertebral foramina at C4/5-Th1/2 in the median and ulnar nerves, we used a dataset for the median nerve from a previous study (Sumiya et al., 2017). The relative intensity of currents to the largest current that flowed through the intervertebral level at the stimulated sides were calculated for each participant, and those after median nerve stimulation (n = 20) were compared with those after ulnar nerve stimulation (n = 20) using a *t*-test with post-hoc test.

3. Results

3.1. Magnetic field signals

Before removal of stimulation artifacts, neuromagnetic fields in earlier latent phases were not observed in 6 of 20 nerves after wrist stimulation and were not observed in all 20 nerves after elbow stimulation because electrical stimulation-induced artifacts overlapped with signals until about 10 ms after stimulation (Fig. 2a). After artifact removal, cervical nerve evoked magnetic fields could be observed from early latent phases in all cases (20 nerves in 10 participants) (Fig. 2b).

The magnetic field signals showed 2–4 phasic waveforms, similar to those of evoked magnetic fields after median nerve stimulation reported previously (Sumiya et al., 2017). The mean amplitude and latency of the maximum peak of the Y-axis sensor, which are considered to represent the depolarization of spinal nerve fibers, were 30 ± 7.8 fT and 11.5 ± 0.8 ms with wrist stimulation and 64 ± 12.0 fT and 7.5 ± 0.4 ms with elbow stimulation, respectively (Fig. 3).

3.2. Current distribution map

Current distribution maps revealed three current components with either wrist or elbow stimulation (Fig. 4). The first component was the leading component of the intra-axonal current, which flowed mainly into the C6/7-Th1/Th2 intervertebral foramina at 10.2 ± 0.9 ms after wrist stimulation and 6.4 ± 0.4 ms after elbow stimulation on average, and then ascended in the spinal canal (Fig. 4; black asterisks). The second component was the trailing component of the intra-axonal current, which flowed after the leading component into the intervertebral foramina at 11.6 ± 0.9 ms after wrist stimulation and 7.4 ± 0.5 ms after elbow stimulation on average, and propagated along the course of nerves (Fig. 4; light blue asterisks). The third component was inward currents flowing perpendicularly to the course of nerves between the leading and the trailing components and propagated cranially on the convex side of the nerves and outside the spinal canal (Fig. 4; black stars). The mean latency for the inward currents propagating through the C5 level was 12.0 ± 0.9 ms after wrist stimulation and 8.0 ± 0.4 ms after elbow stimulation. The current intensity after elbow stimulation was about twice that after wrist stimulation.

3.3. Calculated current waveforms at the virtual electrode

In our previous study using MSG, we noted that the waveforms from virtual electrodes on the stimulation side (Fig. 5; white asterisks) represented intra-axonal currents of the nerve roots flowing into the intervertebral foramina while those from the contralateral side (Fig. 5; black asterisks) represented inward currents at the depolarization site ascending in the spinal canal (Sumiya et al., 2017).

With wrist stimulation, the waveforms of inward currents at the depolarization site ascending in the spinal canal were obtained with good S/N ratios (3 or higher) from Th1/2 up to C5/6 in 18 of 20 nerves (90%), with only 8 of the 20 nerves (40%) providing good S/N ratios up to C4/5. With elbow stimulation, the corresponding waveforms were obtained with good S/N ratios from Th1/2 up to

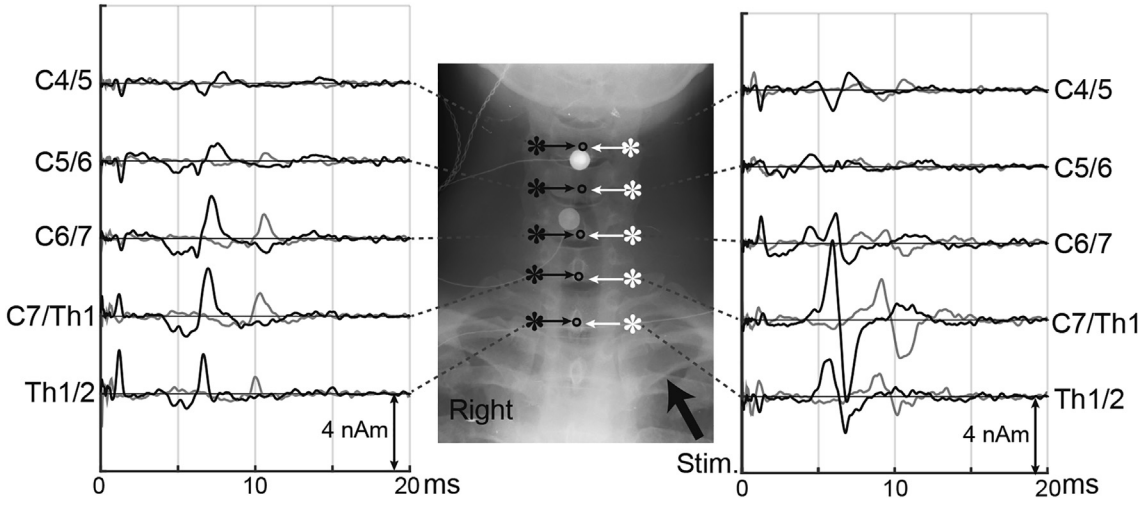

Fig. 5. Calculated current waveforms at virtual electrodes. Virtual electrodes were set 20 mm lateral from the midline of the spinal canal. Black waveforms are calculated currents in response to stimulation of the ulnar nerve at the elbow and gray waveforms are those from stimulation at the wrist. The upward waveform shows the current flowing toward the midline from the virtual electrode. Waveforms of virtual electrodes (white asterisk) on the ipsilateral side of the stimulation indicate the current flowing into the intervertebral foramina. Waveforms of virtual electrodes (black asterisk) on the contralateral side of the stimulation indicate the ascending inward currents at the depolarization site. Neural currents in response to the elbow stimulation (black waveforms) have faster latency, larger amplitude, and a higher S/N ratio than those in response to wrist stimulation.

C5/6 in all nerves (100%) and up to C4/5 in 17 of 20 nerves (85%) (Fig. 5). The conduction velocity between the C5 and C7 levels was 73.4 ± 19.6 m/s, as determined from the peak latency of inward currents at the depolarization site after elbow stimulation.

3.4. Comparison with somatosensory evoked potentials

The peak latency of SEP recorded as the C5 posterior-anterior montage after ulnar nerve stimulation at the elbow, which corresponds to N11 after median nerve stimulation at the wrist, could be determined in 17 nerves.

The peak latency of SEP corresponding to N11 was largely consistent with that of inward currents calculated from MSG at the C5 level (Fig. 6a). Linear single regression analysis showed a high correlation (r = 0.92) (Fig. 6b).

3.5. Individual variations in peak currents flowing into the intervertebral foramina

The peak intensity of the trailing intra-axonal current flowing into the intervertebral foramina at C4/5-Th1/2 was calculated and plotted for 20 nerves of all 10 healthy volunteers (Fig. 7). After

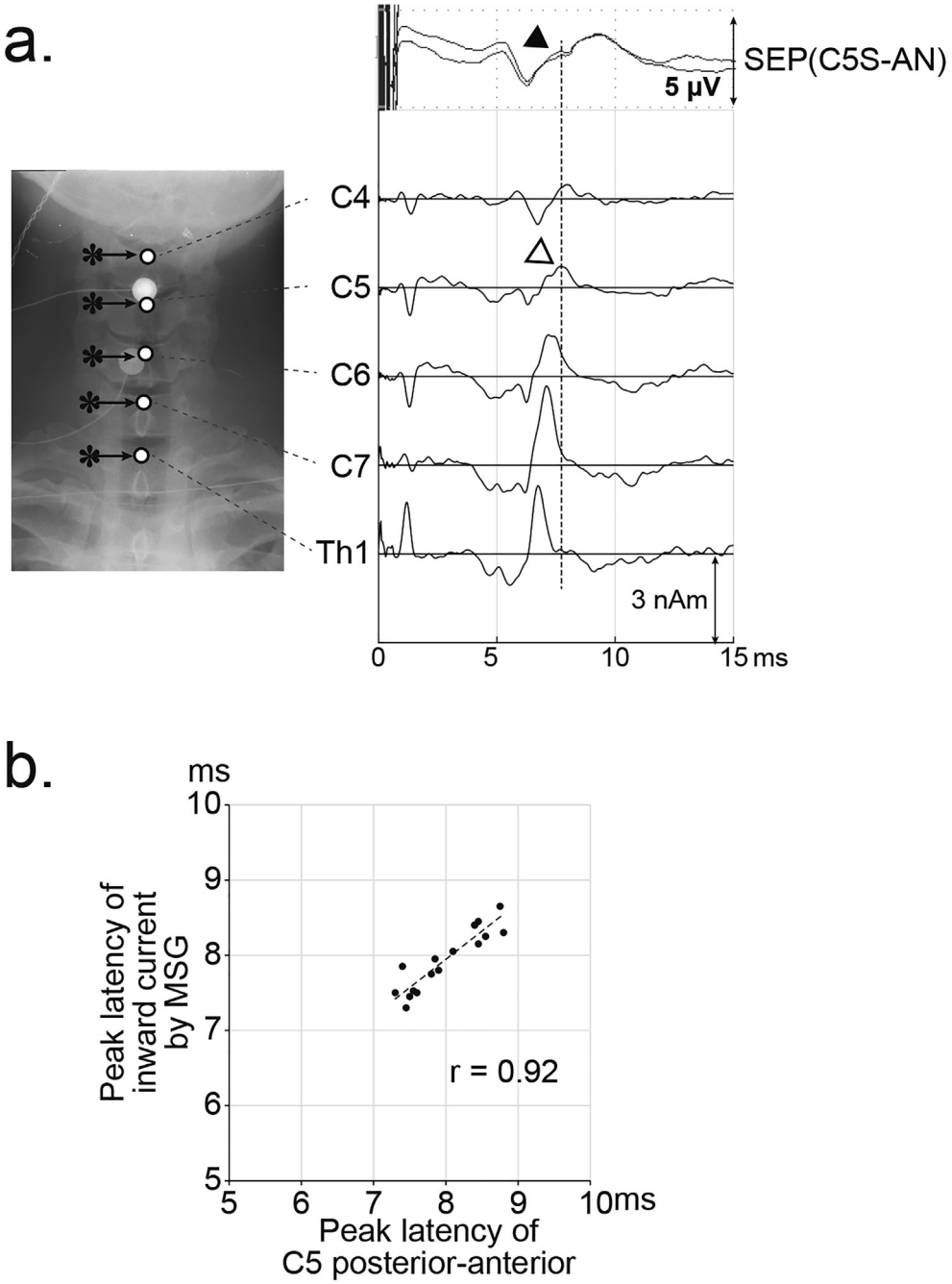

Fig. 6. Correlation between magnetospinography (MSG) and somatosensory evoked potentials (SEP). (a) Waveforms of calculated currents from MSG and SEP. Lower waveforms are the calculated inward currents from MSG at the C4-Th1 vertebral level in response to ulnar nerve stimulation at the elbow. The upper wave is SEP recorded by C5 posterior-anterior montage. Peak latency of SEP (corresponding to N11 in SEP after median nerve stimulation at the wrist) coincided with peak latency (▷) of inward current calculated from MSG at the C5 level. (b) Correlation between peak latency of inward current from MSG and SEP at the C5 level. The peak latency of the calculated inward current at the C5 level and SEP recorded with C5 posterior-anterior montage matched well across 17 participants (r = 0.92).

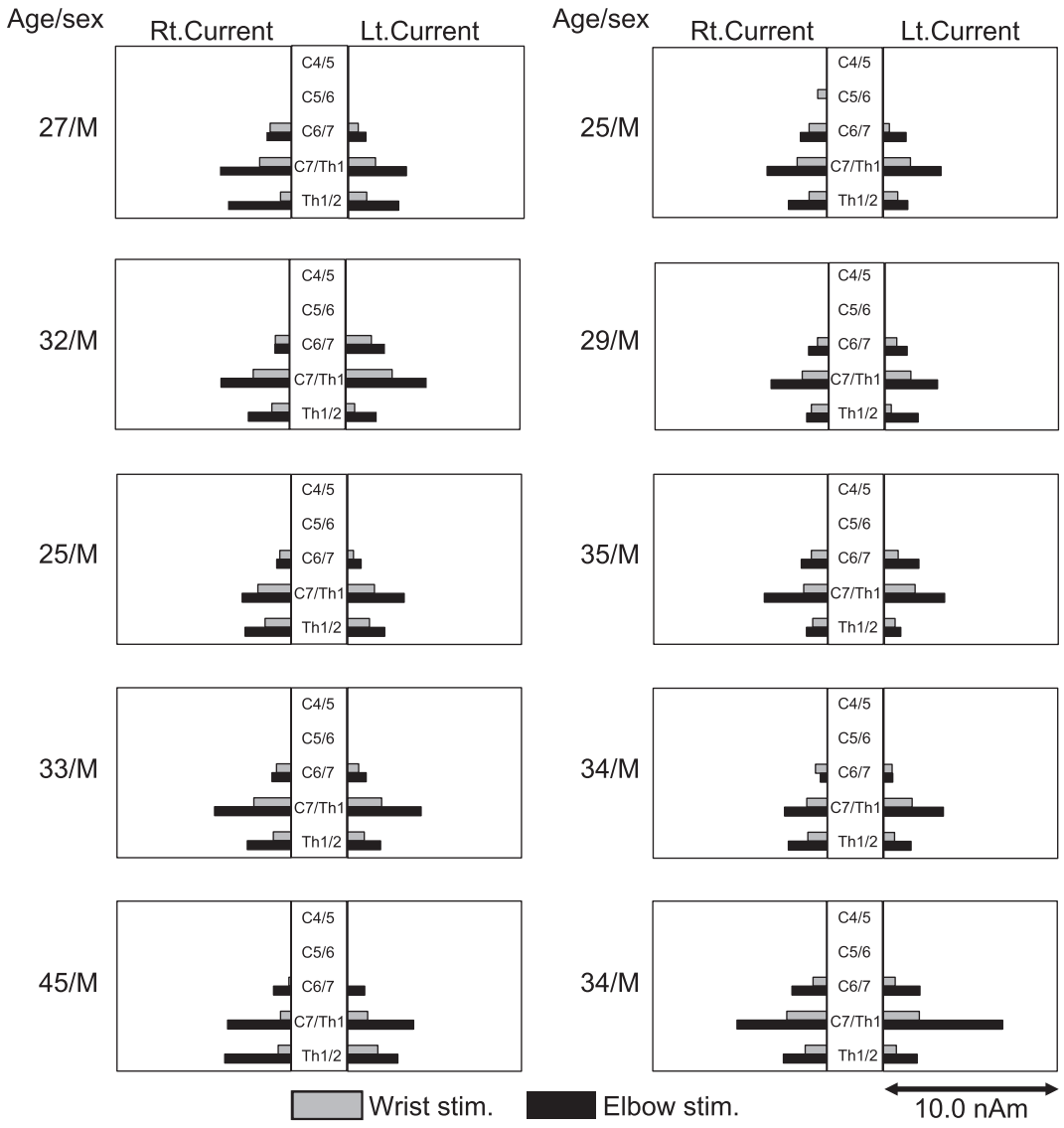

Fig. 7. Spatial distribution of the peak intensity of the trailing intra-axonal current following wrist and elbow stimulation of right and left ulnar nerves in 10 participants. The intra-axonal current after ulnar nerve stimulation mainly flowed into the C6/7-T1/2 level, and the C7/T1 current was the largest in most participants. The current distributions after elbow stimulation and wrist stimulation were similar, but the current intensity after elbow stimulation was about twice that after wrist stimulation.

ulnar nerve stimulation, electrical currents flowed mostly into C6/7-T1/2, with the peak intensity recorded at C7/T1. The mean current intensity after wrist stimulation was 0.72 ± 0.31 nAm, 1.70 ± 0.45 nAm, and 0.94 ± 0.34 nAm at C6/7, C7/T1, and T1/2, respectively, while that after elbow stimulation was 1.25 ± 0.51 nAm, 3.81 ± 0.96 nAm, and 2.18 ± 0.75 nAm, respectively. Foraminal current at C5/6 was present in only 1 of 20 nerves after wrist stimulation, whereas foraminal current at C4/5 was not observed in any nerve.

The correlation coefficient between the current intensity flowing into the intervertebral foramina after wrist stimulation and that after elbow stimulation was 0.91 ([Current after elbow stim.] = 2.03 * [Current after wrist stim.] + 0.076, $p < 0.01$), indicating a high level of correlation and a similar pattern of current distribution.

When comparing the distribution of currents flowing into the intervertebral foramina after ulnar nerve stimulation at the elbow with that after median nerve stimulation, relative intensity of the current flowing into the C5/6 and C6/7 foramina was significantly lower after ulnar nerve stimulation ($p < 0.001$) (Fig. 8).

4. Discussion

4.1. Efficacy of artifact removal method

Before artifact removal, stimulation artifacts overlapped with early neuromagnetic field signals in 30% of cases after wrist stimulation and in all cases after elbow stimulation, where the site of stimulation was closer to the recording site, making it difficult to estimate the source of signals. These stimulation artifacts were adequately removed in all cases using the DSSP method (Sekihara et al., 2016). In a previous study on MSG after median nerve stimulation reported by Sumiya et al., artifacts were removed using the common-mode subspace projection (CSP) method (Sekihara et al., 2017), which requires not only evoked neuromagnetic field data after median nerve stimulation, but also data for stimulation artifacts alone (Sumiya et al., 2017). The DSSP method used in the present study does not require data for stimulation artifacts alone, and thus requires a shorter total measurement time and provides a greater advantage for clinical application compared with the CSP method.

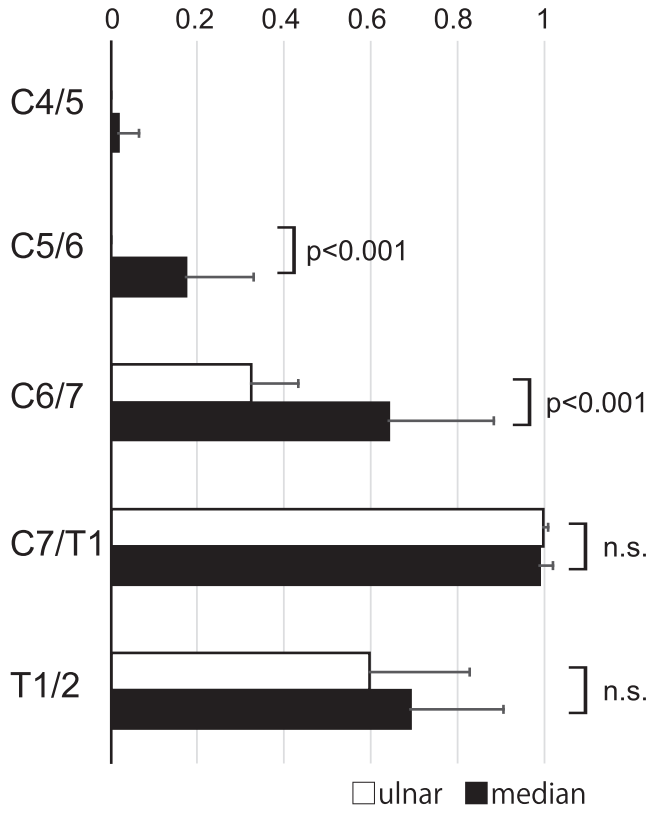

Fig. 8. Comparison of the distribution of the currents flowing into the intervertebral foramina after ulnar nerve stimulation at the elbow and after median nerve stimulation (Sumiya et al., 2017). The relative intensity of the current flowing into the C5/6 and C6/7 foramina was significantly lower after ulnar nerve stimulation.

4.2. Characteristic of MSG in response to ulnar nerve stimulation

Current distribution maps revealed three current components, namely, the leading and trailing components of the intra-axonal current and inward currents between them, which propagated cranially by flowing through the intervertebral foramina into the spinal canal, after either wrist or elbow stimulation. The conduction velocity between the C5 and C7 levels was 73.4 ± 19.6 m/s, which was physiologically relevant. This result was consistent with the value obtained by MSG after median nerve stimulation (73.0 ± 15.8 m/s) (Sumiya et al., 2017).

After ulnar nerve stimulation, intra-axonal currents flowed mainly into the C6/7-T1/2 intervertebral foramina, which is consistent with the anatomical finding that the ulnar nerve contributes to the C7-T1 nerve roots (Sinha et al., 2016). Anatomically, only C8/T1 root innervation is thought to contribute to ulnar nerve stimulation at the wrist, with additional contribution from C7 root innervation of the flexor carpi ulnaris to elbow stimulation (Standring et al., 2008). Although foraminal current at C6/7 (C7 root innervation) was observed in 19 nerves and C5/6 (C6 root innervation) was observed in 1 nerve after wrist stimulation (Fig. 7), further studies, including animal experiments, are needed to confirm this finding because the accuracy of signal source estimation by the spatial filtering method may not be sufficient. The absence of movement in the hand muscles innervated by the median nerve was confirmed with the unaided eye, but the possibility of co-stimulation of the median nerve during stimulation at the wrist cannot be eliminated.

In sum, the present measurement and signal processing methods enabled visualization of neural activities in the nerve roots and spinal cord after ulnar nerve stimulation. The peak latency of SEP corresponding to N11 recorded as C5 posterior-anterior montage was largely consistent with the peak latency of inward currents calculated from MSG at the C5 level, suggesting that neural activity in the posterior column of spinal cord can be measured with high spatial resolution based on inward currents recorded by MSG.

4.3. Comparison of wrist stimulation and elbow stimulation

Mackert et al. (2001) reported conductive magnetic fields in the cervical nerve roots after ulnar nerve stimulation at the wrist, but the evoked signals were small (10 fT). Elbow stimulation is theoretically advantageous because it involves stimulation of more nerve fibers and is less affected by dispersion due to the shorter interval from stimulation to recording compared with wrist stimulation. At the same time, because the neuromagnetic fields in response to stimulation at the elbow have greater overlap with stimulation artifacts, clinical application has been difficult. In this study, the introduction of the artifact removal method could enable practical use of MSG with elbow stimulation.

The signal intensity of the measured magnetic field with elbow stimulation was approximately twice that with wrist stimulation, making it possible to estimate the signal source from data with a good S/N ratio. Current waveforms were acquired with good S/N ratios up to the C4/5 level in 40% with wrist stimulation and 85% with elbow stimulation, demonstrating the superiority of elbow stimulation. While electrical currents flowing into the intervertebral foramina also showed a similar distribution pattern between wrist and elbow stimulation, a 2-fold higher current intensity was recorded with the latter, suggesting that elbow stimulation is more suitable for clinical application.

4.4. Comparison with median nerve stimulation: Advantages and disadvantages

This study showed that the relative intensity of the current flowing into the C5/6 and C6/7 foramina was significantly higher after median nerve stimulation than after ulnar nerve stimulation (Fig. 8). This does not contradict previous findings that the roots contributing to the median nerve are located in more cranial segments (Sinha et al., 2016).

Since the uppermost nerve roots forming the median nerve are at the C5 (C4/5) level, electrical currents ascending along the posterior column of spinal cord and those in the nerve roots are mixed at C5/6 and lower levels making it difficult to detect abnormalities in the posterior column of the spinal cord. By comparison, the C7 nerve roots (at C6/7) are the uppermost roots forming the ulnar nerve, making ulnar nerve stimulation more advantageous for detecting abnormalities in the posterior column at C5/6/7 or lower levels.

Taken together, MSG with median nerve stimulation should be used for the diagnosis of C5 or C6 radiculopathy or abnormalities in the posterior column at C4/5 or higher levels while MSG with ulnar nerve stimulation should be used for examining the posterior column at the C5/6/7 levels.

5. Conclusion

Using cervical MSG with ulnar nerve stimulation, we successfully visualized neural activities flowing into the intervertebral foramina at the C6/7-T1/2 levels and ascending in the spinal canal. Our data suggest that ulnar nerve stimulation is more effective than median nerve stimulation for the diagnosis of spinal cord disorders at C5/6/7, because ulnar nerve stimulation results in neural activity flowing into lower cervical vertebral levels. Moreover, in

MSG measurements, elbow stimulation produces more intense signals than wrist stimulation and thus is more advantageous for clinical application.

Funding

This research did not receive any specific grant from funding agencies in the public, commercial, or not-for-profit sectors.

Author contributions

Y. Miyano, S. Kawabata, M.A., and A.O. took part in the conception and design of the project; Y. Miyano, S. Kawabata, T.S., T.W., S. Kim, S.S., Y. Mitani, and Y.A. were involved in its execution; and Y. Miyano. S. Kawabata., M.A., T.W., K.S. and Y.A. performed analysis and interpretation of data. All authors have approved the submission of this manuscript.

Declaration of Competing Interest

The authors declare that they have no known competing financial interests or personal relationships that could have appeared to influence the work reported in this paper.

References

Adachi Y, Kawai J, Haruta Y, Miyamoto M, Kawabata S, Sekihara K, et al. Recent advancements in the SQUID magnetospinogram system. Supercond Sci Technol 2017;30:063001.

Bednarik J, Kadanka Z, Dusek L, Kerkovsky M, Vohanka S, Novotny O, et al. Presymptomatic spondylotic cervical myelopathy: an updated predictive model. Eur Spine J 2008;17:421–31.

Ishii S, Kawabata S, Tomizawa S, Tomori M, Sakaki K, Shinomiya K, et al. Conductive neuromagnetic fields in the lumbar spinal canal. Clin Neurophysiol 2012;123:1656–61.

Kumihashi I, Sekihara K. Array-gain constraint minimum-norm spatial filter with recursively updated gram matrix for biomagnetic source imaging. IEEE Trans Biomed Eng 2010;57:1358–65.

Mackert BM, Burghoff M, Hiss LH, Nordahn M, Marx P, Trahms L, et al. Magnetoneurography of evoked compound action currents in human cervical nerve roots. Clin Neurophysiol 2001;112:330–5.

Matsumoto M, Fujimura Y, Suzuki N, Nishi Y, Nakamura M, Yabe Y, et al. MRI of cervical intervertebral discs in asymptomatic subjects. J Bone Joint Surg Br 1998;80:19–24.

Nagata K, Yoshimura N, Hashizume H, Muraki S, Ishimoto Y, Yamada H, et al. The prevalence of cervical myelopathy among subjects with narrow cervical spinal canal in a population-based magnetic resonance imaging study: the Wakayama Spine Study. Spine J 2014;14:2811–7.

Nakashima H, Yukawa Y, Suda K, Yamagata M, Ueta T, Kato F. Abnormal findings on magnetic resonance images of the cervical spines in 1211 asymptomatic subjects. Spine (Phila Pa) 1976;2015(40):392–8.

Sekihara K, Kawabata Y, Ushio S, Sumiya S, Kawabata S, Adachi Y, et al. Dual signal subspace projection (DSSP): a novel algorithm for removing large interference in biomagnetic measurements. J Neural Eng 2016;13:036007.

Sekihara K, Nagarajan SS. Electromagnetic brain imaging: a Bayesian perspective. Springer International Publishing; 2015.

Sekihara K, Nagarajan SS. Subspace-based interference removal methods for a multichannel biomagnetic sensor array. J Neural Eng 2017;14:051001.

Shinomiya K, Furuya K, Sato R, Okamoto A, Kurosa Y, Fuchioka M. Electrophysiologic diagnosis of cervical OPLL myelopathy using evoked spinal cord potentials. Spine (Phila Pa) 1988;1988(13):1225–33.

Sinha S, Prasad GL, Lalwani S. A cadaveric microanatomical study of the fascicular topography of the brachial plexus. J Neurosurg 2016;125:355–62.

Standring S, Ellis H, Healy J, Williams A. Gray's anatomy 40th Edition. Anatomical basis of clinical practice. Churchill Livingstone, London. 2008;40:415.

Sumiya S, Kawabata S, Hoshino Y, Adachi Y, Sekihara K, Tomizawa S, et al. Magnetospinography visualizes electrophysiological activity in the cervical spinal cord. Sci Rep 2017;7:2192.

Tamaki T, Kubota S. History of the development of intraoperative spinal cord monitoring. Eur Spine J 2007;16(Suppl 2):S140–6.

Tani T, Ishida K, Ushida T, Yamamato H. Intraoperative electroneurography in the assessment of the level of operation for cervical spondylotic myelopathy in the elderly. J Bone Joint Surg Br 2000;82:269–74.

Ushio S, Hoshino Y, Kawabata S, Adachi Y, Sekihara K, Sumiya S, et al. Visualization of the electrical activity of the cauda equina using a magnetospinography system in healthy subjects. Clin Neurophysiol 2018;130:1–11.